Early warning sensors for monitoring mercury in water

U. Pinaeva, D. Lairez, O. Oral, A. Faber, M-C. Clochard, T.L. Wade, Pauline Moreau, Jean Philippe Ghestem, M. Vivier, S. Ammor, et al.

Early Warning Sensors for Monitoring Mercury in Water

U. Pinaeva[1], D. Lairez[1,2], O. Oral[1], A. Faber[1], M-C. Clochard[1], T. L. Wade[1], P. Moreau[3], J-P. Ghestem[3], M. Vivier[4], S. Ammor[4], R. Nocua[5] and A. Soulé[5]

[1]Laboratoire des Solides Irradiés, CNRS-CEA-Université Paris-Saclay, UMR7642, Ecole polytechnique, 91128 Palaiseau Cedex, France
[2]Laboratoire Léon Brillouin, CNRS-CEA-Université Paris-Saclay, CEA-Saclay, 91191 Gif-sur-Yvette Cedex, France
[3]BRGM, 3 avenue Claude-Guillemin, BP 36009, 45 060 Orléans, France
[4]SGS France, Technopole du Madrillet, 65 rue Ettore Bugatti, BP 90014, 76 801 St-Etienne du Rouvray Cedex, France
[5]VALOTEC, Villejuif Bio Park, 1 mail du Professeur Georges Mathé, 94 800 Villejuif, France

April 30, 2020

Abstract

Poly-4-vinylpyridine grafted poly(vinylidene difluoride) (P4VP-g-PVDF) nanoporous polymer electrodes were found to be sensitive for Hg(II) analysis. The fabrication and characterization of functionalized nanoporous membrane-electrodes by FESEM and FTIR are presented. Functionalized nanopore charge state versus a large range of pH (1 to 10) was investigated by registering the streaming potential. This isoelectric point is achieved at the pKa of P4VP (pH= 5). Mercury adsorption at solid-liquid interface obeys a Langmuir law. A protocol for accurate Hg(II) analysis at ppb level was established. Calibration curves were performed and different real water samples (mineral water, ground water, surface water) were spiked and analyzed. The resulting sensor is intended to be integrated into existing systems or used standalone as portable devices. A first generation prototype exhibiting its own integrated potentiostat, its software and set of membrane-electrode pads is presented.

KEYWORDS: Mercury, Anodic Stripping Voltammetry, Membranes, Nanopores, Radiografting

1 Introduction

The need for water quality monitoring, in different environmental and health context required by european and national regulations, is increasing. It gives rise to large sampling campaigns with spot sampling, handling, preserving, shipping, storing samples and then time consuming laboratory analysis. The trend for some applications is toward real-time, on-site or *in situ* analyses to improve the reliability of monitoring regarding, for example, the representativity of sampling, faster information and increasing the capacity of real time warning systems. Quality standards are now in the very low μg/L (ppb) or ng/L range. The objective of getting on site or *in situ* information requires fast, portable, low-cost, environmentally friendly and sensitive instruments; however, few options are available. Among all monitored pollutants, mercury is one of the priority substances identified by the Water Framework Directive (Directive 2000/60/EC) for which discharges have to be stopped before 2020. However, in some historical industrial context or illegal activities (gold panning) mercury contamination subsists. Electrochemical mercury sensors allow *in situ* detection but suffer from a lack of repeatability due to memory effects resulting from the difficult removal of mercury from the working electrode.[1] This serious drawback limits their implementation in standard laboratories. Laboratory analyses are still based on expensive equipments such as atomic adsorption (AAS) or atomic fluorescence spectroscopy (AFS) or inductively coupled plasma mass spectroscopy (ICP-MS).

Based on Anodic Stripping Voltammetry (ASV) detection, our team has already proposed functionalized nanoporous polymer electrodes sensitive and selective for heavy metal analysis.[2] With their 3D nanostructure, which allows *in situ* sampling, these membrane-electrodes are ideal for self-monitoring of metals directly on-site. The manufacturing of these membrane-electrodes is so cheap that they can be used as disposable products. This technology relies on gold coated ion-track etched nano-functionalized membranes made of bio-compatible polyvinylidene fluoride (PVDF). Gold electrodes have already shown a remarkable stability toward Hg(II) ASV determination.[3][4][5] The actual trend for the development of new electrochemical sensors for mercury is the nanostructuration of electrodes as it significantly reduces the Hg(II) detection limit.[6][7][8][9][10] The proposed nanoporous electrodes mix not only the gold electrode nanostructuration but also the functionalization inside of the cylindrical nanopores to collect and pre-concentrate Hg(II) ions by passive adsorption. Poly-4-vinyl pyridine (P4VP), well-known to complex heavy metals such as Cu(II), Co(II), Cr(VI), [11][12][13] has a special affinity for Hg(II).[14][15][16] The pyridinium cycle therefore boots Hg(II) preconcentration.[17] The selectivity for mercury ions was also reported for P4VP grafted PVDF track-etched membranes.[18] The resulting sensors measure mercury well below the limitations imposed by existing norms for landfill and soil leachate. In this field, there is a need for portable and reliable non-certified sensors which can act as early warning sensors to alert in the case of pollution events. The sensors should warn if the mercury level in soil leachate exceeds a threshold of 200 ppb from class 2 non dangerous to class 2 dangerous and 10 ppb from class 2 non dangerous to class 3 inert -EU directive of the 15 march 2006-) making them competitive. Nevertheless, considering the ability of mercury for non-specific adsorption on solid surfaces,[20] the understanding of mercury adsorption at the solid-liquid

interface inside the P4VP functionalized nanoporosity has to be studied. As the objective is to integrate these Hg(II) sensors in a portable device, the establishment on a robust protocol to obtain reliable results is necessary.

To address these issues, the present publication reports not only on the fabrication and characterization of functionalized nanoporous P4VP-g-PVDF membranes-electrodes by Field Emission Scanning Electron Microscopy (FE-SEM) and Fourrier transformed infra-red (FTIR), but also, on functionalized nanopore charge state versus a large range of pH (1 to 10). The latter study was performed by registering the streaming potential through the nanopores. To go deeper in the understanding of mercury adsorption at solid-liquid interface, a Langmuir model was investigated. A protocol for mercury analysis at ppb level using these innovative disposable membrane-electrodes has been determined. A performance evaluation on a set of natural water samples was also performed to look at possible interferences. Finally, a first generation prototype exhibiting its own integrated potentiostat, its software and a set of single-use membrane-electrode pads is herein presented.

2 Materials and methods

2.1 Irradiation

Bi-oriented and polarized PVDF films were purchased from PIEZOTECH SA (thickness: $9\mu m$). Swift Heavy Ions (SHI) irradiations were performed at GANIL, France. Films were irradiated at room temperature with Xe^{54+} at energy of 5.9 MeV.amu^{-1} under He atmosphere. Fluence was equal to 10^9 cm^{-2}.

2.2 Track-etching

Chemical attack is performed at 65°C in a solution of KOH 10 N and $KMnO_4$ 0.25 N. The final diameter depends on the etching time. To obtain a pore diameter of 50 nm, 30 minutes of etching were required. Afterwards, etched PVDF films were first washed in potassium disulfite solution (15 %) and then 3 times rinsed with deionized water.

2.3 Radiografting and gold sputtering

Remaining radicals present in the pore walls were used to initiate a radical polymerization in presence of 4-vinylpyridine following a reported method.[18] 4-vinylpyridine was purchased from Sigma-Aldrich without further purification. Pure liquid 4-vinylpyridine monomer solution was added. A bubbling under nitrogen gas was performed for 15 min before radiografting. The radiografting reaction temperature was set at 65°C. Reaction time was 15 min. The resulting P4VP-g-PVDF nanoporous membranes were rinsed in deionized water, then immersed in ethanol. Finally, they were put in HCl solution at pH 2 for 48 h. The membranes were dried gently at room temperature for 24h.
A gold layer of 35nm was sputtered on both side of the nanoporous membrane through a mask to form membrane-electrodes. The design of the mask was

adapted to the electrochemical probe which was shaped as a clip for practical use. A circular electrode was preferred to fit with the demonstrator clip (two dimensions were used 4 mm and 8 mm of diameter) while a square one (1 cm^2) was more appropriate according to prototype pad design.

2.4 Zeta potential measurements

The flow of water through porous membranes comes with the flow of ions in solutions. In case pore-walls are electrically charged, the global electric neutrality necessarily implies that the flowing solution is not neutral, but contains an excess of charges of opposite sign to that of the pore-walls. Thus, the liquid flow causes an electric current named streaming current. In the framework of: 1) the Gouy-Chapman-Stern theory for the electric double-layer that neutralizes the surface; and 2) the Poiseuille's law for laminar flow; one obtains for the streaming current I_{str}:

$$I_{\mathrm{str}} = -\zeta\epsilon\frac{\pi r^2 \Delta P}{\eta l} \tag{1}$$

where ϵ is the electric permittivity, r the hydrodynamic radius of the pore, l its length, η the viscosity of the solution, ΔP the difference of hydrostatic pressure between the two extremities of the pore and ζ (zeta) the electric potential at a distance from the pore-wall at which the fluid velocity becomes zero. Equation 1 cannot be directly used to measure ζ, e.g. by measuring I_{str} as a function of ΔP, because the current would be cancelled by the potential U_{str} due to the accumulation of charges it produces itself: $U_{\mathrm{str}} = I_{\mathrm{str}}/G$, where $G = \sigma\pi r^2/l$ is the pore conductance and σ the conductivity of the solution. With Eq.1 one gets

$$U_{\mathrm{str}} = -\zeta \times \frac{\epsilon \Delta P}{\sigma\eta}, \tag{2}$$

where all geometric parameters vanish. It is actually this potential that is measured by applying a feedback transmembrane voltage $U = -U_{\mathrm{str}}$ allowing the electric current to be maintained at zero once a pressure diffrence ΔP is applied. From the slope of U versus ΔP, one gets ζ for a salt solution with known σ, η and ϵ.

Measurements were performed by means of a home made device. The membrane is trapped between two compartments with Ag/AgCl electrodes and containing a 0.1 M KCl solution. One compartment experiences a varying pressure coming from a syringe-pump, whereas the other remains at the atmospheric pressure. The pressure difference ranging between ± 0.3 bar is measured with a differential-pressure transducer whereas the feedback voltage is automatically applied, and so measured, using an Axopatch-200B amplifier working in the "I=0" mode.

2.5 ASV measurements

Once Au-sputtered, functionalized track-etched P4VP-g-PVDF nanoporous sensors were put in Hg(II)-spiked aqueous solutions for adsorption. For adsorption/exposition tests, the sensors were immersed in Hg(II)-spiked aqueous solutions. Adsorption was passive meaning that application of potential was not needed. During adsorption step, orbital shaker or ping-pong stirrer (250 rpm)

were used for stirring Hg(II) polluted solutions. During this step, solvated mercury ions were preconcentrated inside the P4VP functionalized nanopores.

2.5.1 Exposition of the sensors to tested waters (natural and spiked)

Atomic Absorption Spectroscopy stock solution of Hg(II) (1g/L) was purchased from Alfa Aesar. Nitric acid (65%) and NaCl were purchased from Sigma-Aldrich. For calibration, dilutions in milliQ water were realized in volumetric flasks to obtain final concentrations of 0.5, 1, 2, 5 ppb. For real samples analysis, an intermediate dilution was prepared in volumetric flask in milliQ water and a final dilution was performed in a 250 mL volumetric flask using tested water. Exposition of each membrane-electrode was performed with the same protocol for calibration and real samples analysis: one membrane-electrode (also called sensor) was added in glass containers of 125 mL, 2/3 filled with the tested solution. The flasks were closed and agitated for 4h at room temperature (20±5°C) otherwise specified. For each condition (concentration, water type) 3 replicates of each flask were prepared. 12 real water samples have been used for recovery tests: 2 bottled mineral waters (MW), 3 ground waters (GW) and 7 river waters (SW). GWs and SWs were sampled in France, in different locations. 2 ppb of mercury was added to each sample. The final concentration of mercury in spiked waters was monitored by Atomic Fluorescence Spectroscopy (AFS) applying NF EN ISO 17852. The preparation of the solutions and the analysis of the sensors were done simultaneously with a calibration curve. One trial was performed at lower temperature in milliQ water. For this trial, the water was left in a refrigerator (4°C) for 1 night before preparing the solutions and the exposition was performed in a cool box

2.5.2 Electrochemical analysis

After exposition of the sensors, they were placed into a voltammetric cell for electrochemical analysis. Square Wave Anodic Stripping Voltammetry (SW-ASV) was used for qualitative determination of adsorbed species. Analysis protocol was established as follows: electrodeposition time of 50 seconds at -0.8 V, voltage scanning from -0.8 V to + 1 V at 75 Hz, 3 mV step and 30 mV amplitude. The electrolyte for the analysis was 10 mM HNO_3 and 10 mM NaCl. Two potentiostats were used for SW-ASV measurements. The first, PalmSens (The Netherlands), completed by a home-made clip device was used for labscale tests. The clip ensured a connection between the membrane-electrode and the potentiostat. Two gold wires were used for contact with gold coated parts of the membrane, silver wire was used as pseudo-reference electrode. The second potentiostat was a first generation prototype device made by ValoTec (France). A special pad was used for strongly anchoring the membrane-electrode inside ensuring good electrical contact. Sputtered silver electrode was used as pseudo-reference electrode. The pad was then plugged to a pad holder, which was connected to the potentiostat. The design of this prototype was done to allow on-site and *in situ* analyses.

3 Results and discussion

3.1 Fabrication and characterization of functionalized nanoporous membranes

The fabrication steps are summarized in Figure 1. Once the PVDF thin films have been irradiated by swift heavy ions at the desired fluence of 10^9 cm^{-2}(step I), they were chemically etched by a strong alkaline solution containing oxidative species (step II). The ion-track etched PVDF membrane results in a membrane with well-defined cylindrical nanopores (Figure 2). Track-etched PVDF nanopore walls are rich with radicals. These radicals have been created during ion-beam pre-treatment. The radicals, which were located in the crystalline areas, kept trapped and could not diffuse nor recombine [2] Freshly etched PVDF membranes with pore diameters of 60 nm were then immersed in 4-vinyl pyridine (4-VP) monomer solution. Heating the system to 65°C gave sufficient energy to the remaining radicals to initiate the 4-VP polymerization from the pore walls (step III).

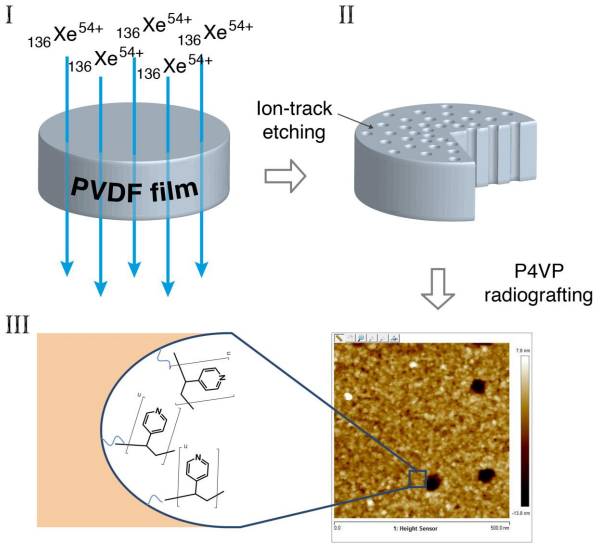

Figure 1: Fabrication steps to create P4VP-g-PVDF nanoporous membrane: I. swift heavy-ion irradiation of PVDF thin film; II. creation of cylindrical nanopore by ion-track etching; III. functionalization by radiografting inside the nanopores; IV. AFM 2D picture of P4VP-g-PVDF nanoporous membrane and scheme of pore interior.

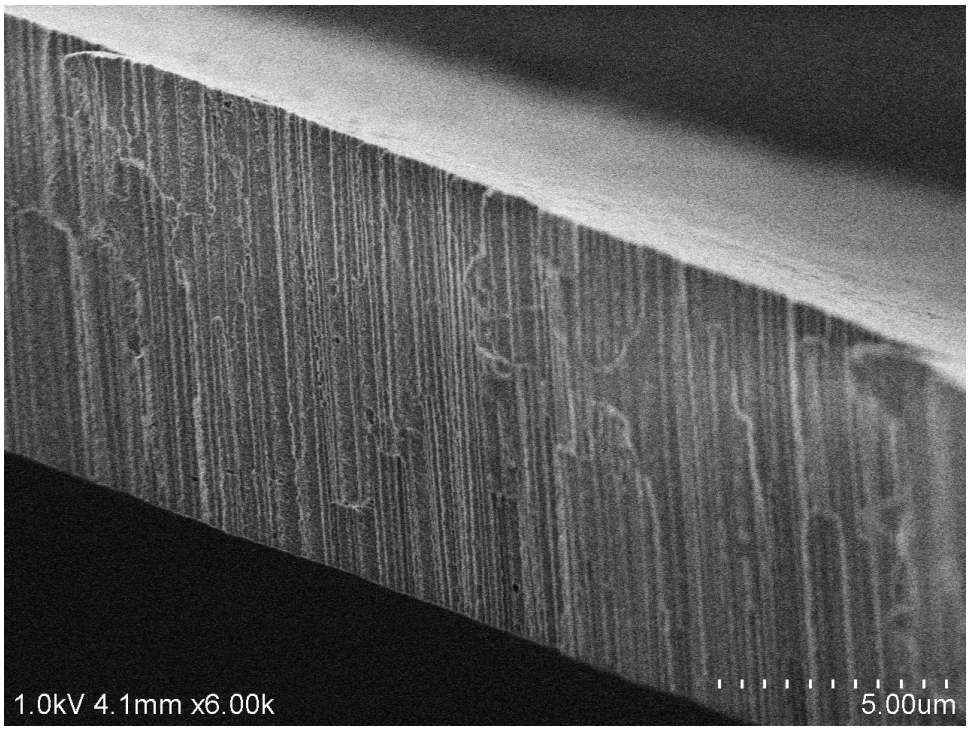

Figure 2: FESEM cryo-section of PVDF track-etched membranes of 10^9 nanopores .cm^{-2} ($Kr^{34+/36+}$ of 10 MeV/mau irradiation performed at GANIL, France)- membrane thickness of 9 μm, pore diameter of 50 nm.

The functionalized P4VP-g-PVDF nanoporous membranes were characterized by FTIR (Figure 3). The FTIR spectrum predominantly exhibits the characteristic absorption bands of PVDF with its doublet corresponding to CH_2 vibrations at 2985 and 3025 cm^{-1}, a multiplet with spectral bands at 1453, 1424, 1403 and 1385 cm^{-1} attributed to a mixture of CH_2 and C-C vibrations, the two most intense bands for CF_2 absorption at 1211 and 1183 cm^{-1} and the PVDF skeleton vibration region between 900 and 400 cm^{-1}. The last region contains well-organized spectral bands. It reflects the conformation of the PVDF chains and gives access to information concerning the crystalline nature. As we have chosen a bi-stretched PVDF film, the signature of β-phase content is shown by the peak presence at 840 cm^{-1}. The pyridinium cycle absorption band at 1600 cm^{-1} (inset of Figure 3) shows the P4VP presence. Its intensity is very small due to the low radio-grafting yield of 1 wt%. The radiografting reaction was intentionally stopped at its early stage (15 min of reaction) to limit the P4VP grafting to the sole pore wall surface and to avoid any pore blockage. The pyridinium cycle displays absorption bands with a main peak at 1600 cm^{-1} surrounded by two satellite peaks at 1560 and 1640 cm^{-1} as previously described.[18] The homogeneity of the grafting on the large treated membranes of 4 x 20 cm^2 was also checked by FTIR comparing the pyridinium cycle absorption band intensity at 1600 cm^{-1} on three very different points.

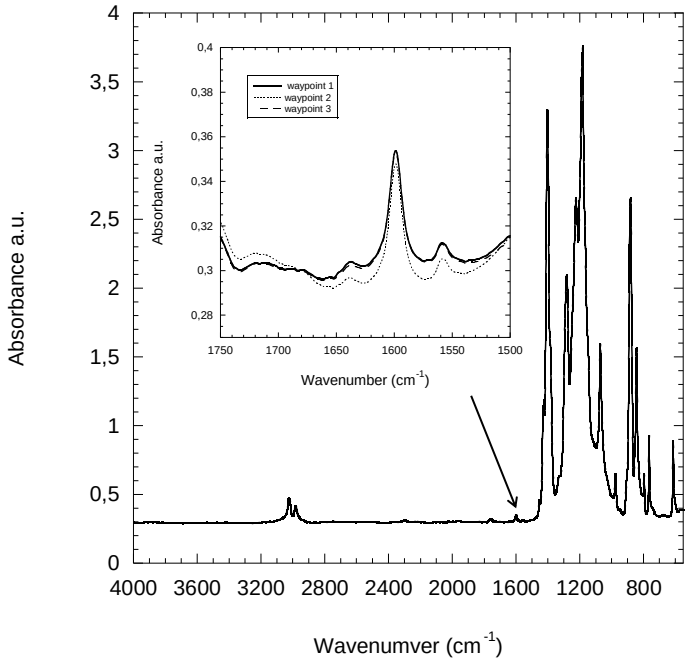

Figure 3: FT-IR spectra in transmission mode of P4VP-g-PVDF nanoporous membrane registered at 3 different points on the same film.

To complete the characterization of grafted P4VP onto the PVDF nanopore walls, we have investigated the quality of the nanopore coverage with P4VP chains by determining the charge state at the solid surface all along the cylindrical nanopores. To do so, a pressure-driven flow of electrolyte solution through the nanopores (or nanochannels) was applied to create an electric streaming current due to the movement of ions in the bulk and electrical double layer at solid-liquid interface. Accumulation of ions downstream generated an electric streaming potential that depends on surface charge, electrolyte concentration, and channel dimensions.[21] With these factors, streaming potential measurements can be used to calculate the zeta potential of pore walls.
Figure 4 displays the zeta potential of P4VP grafted and non-grafted PVDF nanopores. Ungrafted PVDF nanopores were negatively charged. The negative charges correspond to the presence of oxidative species formed at the nanopore surface during the alkaline etching process. The mean zeta potential of -7mV was roughly constant whatever the pH of the solution. P4VP grafted PVDF nanopores exhibited a different behaviour. The nanopore charges were completely inverted into positive charges for very acidic pH. The isoelectric point was reached at pH 5 which corresponds to the pKa of P4VP. [22] It shows that the zeta potential determination *via* the streaming potential is a powerful technique to accurately characterize the charge state of functionalized organic nanopores. It also gives information on the coverage completion of the nanopores walls by the grafted polymer chains. Effectively, the P4VP protonation in acidic

pH was sufficient to completely counterbalance the underneath negative charges of PVDF nanoporous membrane. It means that the grafting coverage is uniform and relatively dense all along the nanopores.

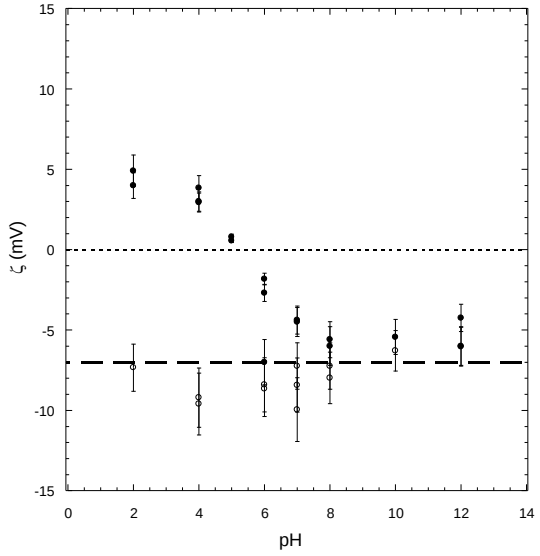

Figure 4: Zeta potential of PVDF nanoporous membranes *against* pH of aqueous solutions. (•) P4VP grafted PVDF nanoporous membrane; (○) non-grafted PVDF nanoporous membrane.

3.2 Mercury detection by ASV

To transform radiografted P4VP-g-PVDF nanoporous membranes into membrane-electrodes, a thin gold layer is sputtered on both membrane surfaces (Figure 5a). The gold layer should be thin enough to not block the pore entry and thick enough to ensure a good conductivity (Figure 5c).

The first step is the passive adsorption of Hg(II) ions by complexation with P4VP functionalities. The membranes were immersed into the Hg(II) solution to analyze for 4h and 24h. The concentration range was 0 to 0.05 μmol.L^{-1} corresponding to 0 to 10 ppb. After adsorption, both gold layers were connected to a potenstiostat. One gold layer served as working electrode and the second one, as counter electrode. The pseudo-reference electrode was made of chlorinated Ag wire. Applied potential of -0.8 V during 50 sec promotes Hg(II) migration to the working electrode, where Hg(II) were reduced into Hg(0). After electrodeposition, a potential scan from -0.8 V to 1V permitted to oxidize again from Hg(0) atoms into Hg(II) ions when reaching Hg(II) redox potential at +0.5V as shown in Figure 5b.

The calibration curves displayed on Figure 5d summarize the mean results obtained from measurements in membrane triplicate of 3 different batches. The obtained calibration shows a deviation from the linearity at 10 ppb. The linearity can be proposed only for a 0 to 5 ppb range. A power curve fit was found

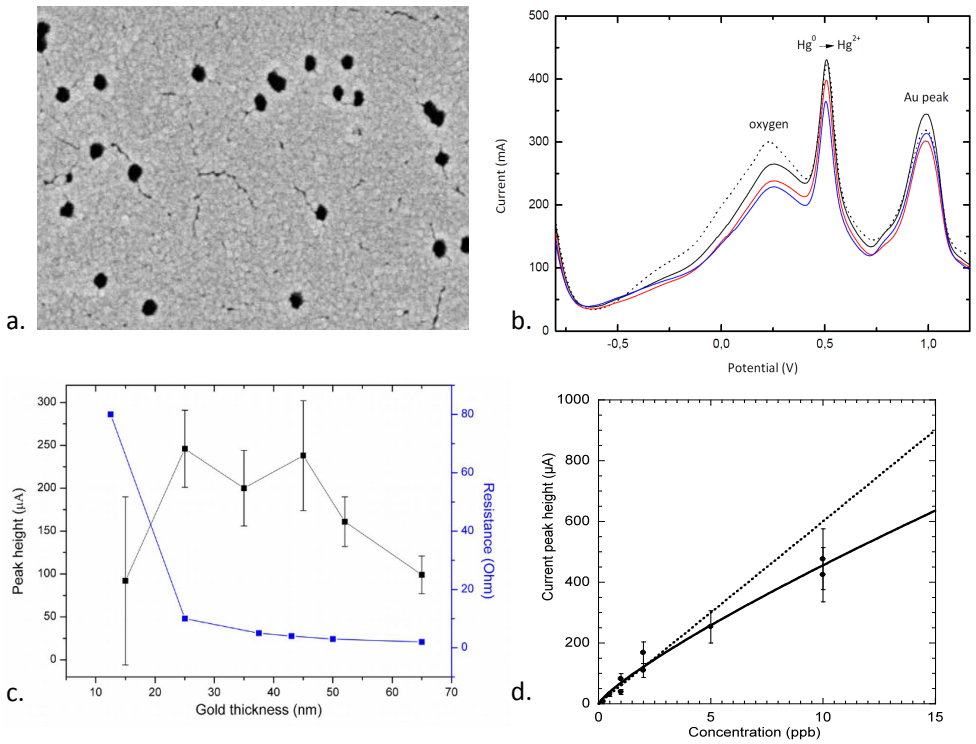

Figure 5: a. FESEM image of the surface of Au-sputtered P4VP-g-PVDF nanoporous membrane; b. ASV voltammograms of Hg(II) adsorbed into P4VP-g-PVDF nanopores - Hg(II) solution concentration of 25 ppb - frequency 25 Hz-, adsorption time of 4h, stirring rate of 250rpm; c. effect of gold layer thickness on the conductivity; d. Calibration curve grouping results obtained on 3 different membrane-electrode batches and registered using circular electrode of 4 mm diameter and pore density of 10^9 cm^{-2} - adsorption time of 4h, stirring rate of 200 rpm - *linear fit:* $y = 60\ x$*; power fit:* $y = 69\ x^{0.82}$.

more appropriate to describe the results considering a larger range (Figure 5d). The mean error of each set of measurements was 21% at 4h of adsorption against 45% at 24h of adsorption (Figure 6).

It was also found that the stirring is of crucial importance for result reproducibility. A ping-pong stirring, set at 200-250 rpm equivalent, gave better results than rotating stirring.

To further explore the sources of error, various calibration curves were performed by three of involved teams from 0.5 to 5 ppb using sensors fabricated at different dates of the year and belonging to 4 different batches of P4VP-g-PVDF membrane-electrodes (Figure 7 left). The calibration curves presented good linearity. However, they could not be superimposed. The variability of peak height might diverge as 2 to 3 times, i.e. for the 5 ppb concentration, the measured current peak heights vary from 35 to 115 μA. Note that the obtained

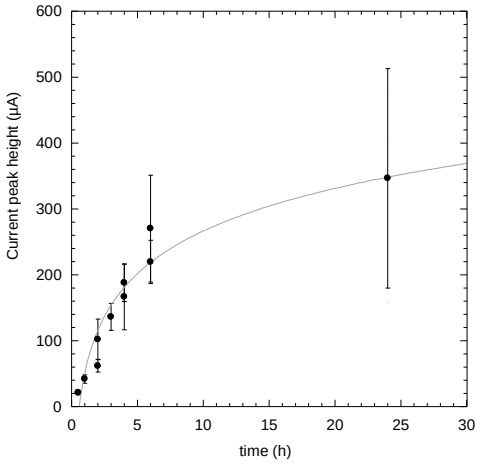

Figure 6: Measured ASV peak height against adsorption time of 2ppb Hg(II) in presence of P4VP-g-PVDF nanoporous membrane; milliQ water, 4 mm circular electrodes, *logarithm fit: y=51.54+215log(x)*

data with the batch 1 showed higher peak heights than those obtained with other batches. This very high sensitivity is sometimes due to a better contact with the demonstrator clip and the Au electrode layer. Considering only batches 2, 3 and 4, the mean values were in the 40-74 μA range.

Taking into account such inter-batch variability, not only triplicates were systematically done for all concentrations and water samples but also, calibration curves were plotted at each analytical sequence with the same batch of membrane-electrodes. As the repeatability for a batch is rather good (20% on average), the user protocol would mention the calibration of the sensor by a three point calibration curve registered the same day.
The effect of temperature was also studied for a given calibration curve (Figure 7 right). A 3 points calibration curve (1, 2, 5 ppb) was performed at 25°C and another at lower temperature (10°C) in MilliQ water. The signal is lower at low temperature. Dispersion seems not to be affected by temperature. This result suggests a thermodynamical equilibrium between Hg(II) and P4VP entities grafted inside the nanopores.

3.3 Sorption of Hg(II) study in P4VP grafted nanopores

To better understand Hg complexation inside P4VP grafted nanopores, we have studied the equilibrium sorption of Hg(II) in aqueous solutions. Experiments were thus carried out at pH 7 on MilliQ solutions of Hg(II) with initial concentrations c_0 ranging from 0.1 ppb to 100 ppb. The measurements were performed at room temperature after 4 hours of P4VP-g-PVDF nanoporous membrane immersion in the Hg(II) solution. The uptake of Hg(II) ions by the P4VP-g-PVDF nanoporous membrane has been evaluated by calculating the variation of Hg(II)

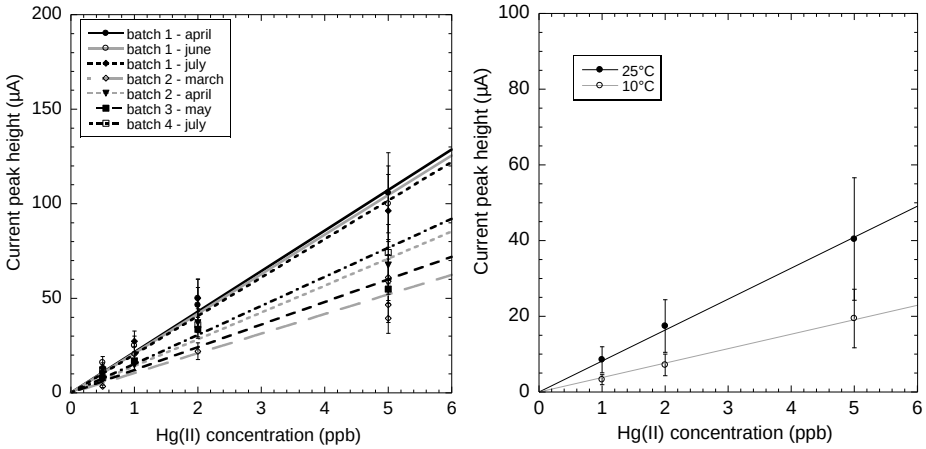

Figure 7: Linear calibration curves for Hg(II) trapped inside P4VP-g-PVDF nanoporous membranes registered using circular electrodes of 8mm diameter and pore density of 10^9 cm^{-2} at : (left) different dates and (right) two temperatures

concentration of the surrounded solution, c_{eq}, before and after membrane immersion. The Hg(II) uptake can be described in the form of sorption isotherm. Figure 8 displays the molar mass q of mercury sorbed at equilibrium per gram of membrane ($mol.g^{-1}$) *versus* the equilibrium concentration c_{eq}. A maximum mass of 0.55 $\mu mol.g^{-1}$ of sorbed Hg(II) was reached. It corresponds to the mercury saturation of the membrane. It is worth noting that the mercury saturation starts at c_{eq} equals to 0.05 $\mu mol.L^{-1}$ corresponding to 10 ppb which explains the observed deviation from the linearity of Hg(II) calibration curves (Figure 5d).
To fit the experimental data, a Langmuir model was used. The Langmuir equation is written as follows (eq. 3):

$$q = \frac{q_{max} b c_{eq}}{1 + b c_{eq}} \tag{3}$$

where q_{max} and b are the maximum sorbed mass at saturation ($\mu mol.L^{-1}$) and the sorption coefficient ($L.\mu mol^{-1}$) respectively. To validate the Langmuir formalism, the linearized form (eq. 4) of eq. 3, known as Hanes-Woolf treatment, was plotted (inset of Figure 8). The thermodynamic equilibrium behaviour is in agreement with previous work [15] for P4VP/Hg(II) complexes at solid-liquid interface.

$$\frac{c_{eq}}{q} = \frac{c_{eq}}{q_{max}} + \frac{1}{bq_{max}} \tag{4}$$

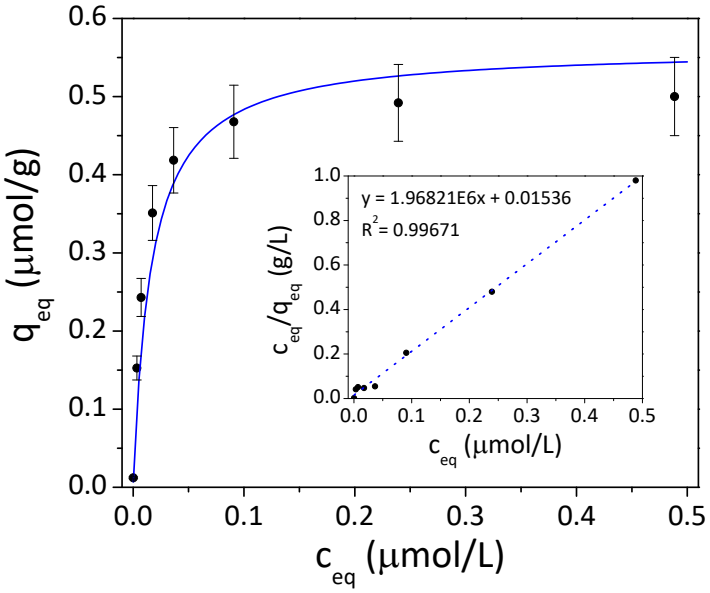

Figure 8: Sorbed Hg(II) concentration *versus* equilibrium concentration: (•) experimental data, (line) Langmuir model; (inset) linearization to assess the Langmuir model towards the experimental data.

3.4 Interference in presence of metal ions and high salt content

In the presence of numerous metallic cations (Ni(II), Zn(II), Cd(II), Cu(II), Mg(II), Pb(II) and Ca(II)), the Hg(II) peak potential did not exhibit any interference (Figure 9a). Neither Hg peak area nor peak height was affected within experimental error, except in presence of Fe(II) ions. The interference with Fe(II) ions confirmed a previous study [18]. It is due to a well-known complex formation between Fe and Hg species in the solution [19]. As a matter of fact, this complex formation decreased the Hg(II) content prior the sorption step by the P4VP-g-PVDF membrane-electrode. The pH effect was already reported in the range from 3 to 9 [18] and no impact on peak intensity was noticed.
The effect of salt content from 0.01 to 35 g.L^{-1} was also investigated (Figure 9b). The concentration of 35 g.L^{-1} of NaCl was herein chosen to simulate seawater. The increase of salt content slightly shifts the Hg peak to more positive potentials. A 0.05V variation of Hg peak potential was observed in salted aqueous solutions from 0.01 to 35 g.L^{-1}. This variation of potential is due to slight fluctuations of the pseudo-reference (chlorinated Ag wire). Such small variations of potential are not a problem as far as the Hg(II) peak height and

area are preserved. An automatic correction was always applied by peak searching mode associated with potentiostat software. These results suggest that the high selectivity of P4VP toward Hg(II) ions allows an Hg detection compatible to seawater environment.

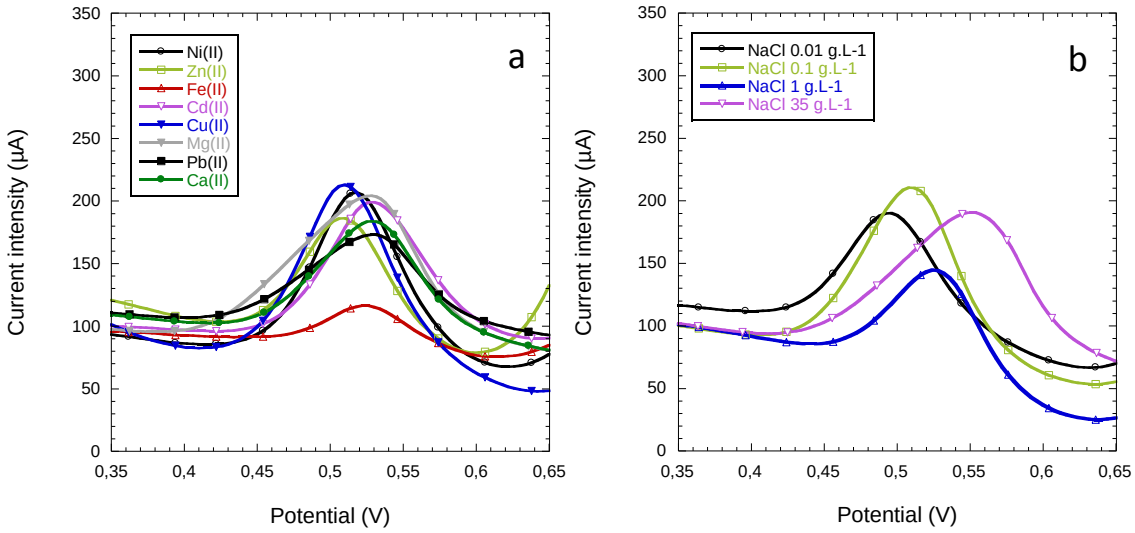

Figure 9: 5 ppb Hg(II) in presence of : 0.1 g.L^{-1} of Ni(II), Zn(II), Fe(II), Cd(II), Cu(II), Mg(II), Cu(II) and 1 mg.L^{-1} of Pb(II) standard solution; b) NaCl at various concentrations: 0.01, 0.1 and 35 g.L^{-1}

3.5 Measurements in natural waters

The results are presented in Table 1 together with natural water samples characteristics such as organic carbon or ion content depending the locations from where these samples were taken (see supplementary information). After adding 2 ppb Hg(II) in water samples, mercury concentrations were both measured by ASV and Atomic Fluorescence Spectroscopy (AFS). Recovery levels were calculated as the ratio of Hg(II) concentrations measured by ASV with the sensor and the total concentration of Hg in the spiked sample measured by AFS. It was shown by ASV that high salt content did not affect mercury adsorption in P4VP-g-PVDF nanoporous membrane-electrodes. The Hg(II) recoveries obtained in the mineral (MW) and ground (GW) waters are higher than 100%,

except for sample GW-3 for which no signal was identified. The latter result was confirmed by a second trial with the same experimental conditions and a different membrane batch. It seems that no interferences occur in mineralized water. In contrast, the Hg(II) recoveries are dramatically decreased when the tests are performed in surface waters (SW). In some SW samples, the signal was totally missing (SW-5 for example). As suspended particulate matters may affect Hg^{2+} sorption, surface water samples were studied as filtrated samples (filter cut-off of 0.7μm) before the trials. In these samples, the recovery is lower than the one obtained in MW and GW samples. It does not seem to be directly correlated to ion content. The effect of dissolved organic carbon content seems more probable as the Hg(II) concentration decreases as dissolved organic carbon increases.

Water type	Suspended matter (mg/L)	Total Organic Carbon (mg/L)	pH	Conductivity (µS/cm)	Measured Hg(II) concentration (ppb)	Recovery* (%)
GW-1	<2	<0.5	7.9	327	3.0 ±0.23	147.6
GW-2	<2	<0.5	7.6	419	3.4 ±0.88	174.0
GW-3	<2	0.8	8.3	597	no peak	no peak
MW-1	<2	-	7.4	-	2.5 ±0.38	138.4
MW-2	<2	0.7	7.2	-	2.7 ±1.61	164.7
SW-1 (filtrated)	<2	0.6	7.8	99	1.3 ±0.44	62.2
SW-2 (filtrated)	<2	1.6	8.1	419	1.6 ±1.28	82.2
SW-3 (filtrated)	<2	3.0	8.4	507	1.0 ±0.38	49.7
SW-4 (filtrated)	<2	3.5	7.5	198	0.1 ±0.07	8.4
SW-5 (filtrated)	<2	4.5	7.8	249	no peak	no peak
SW-4 (raw)	10.0	3.7	7.5	204	0.3 ±0.05	16.7
SW-5 (raw)	8.0	4.8	7.8	249	no peak	no peak
SW-6 (raw)	21.0	4.3	7.5	249	-0.3 ±0.40	0.0
SW-7 (raw)	21.0	9.3	8.2	666	no peak	no peak

* ratio of Hg(II) concentrations measured by ASV and by Atomic Fluorescence Spectroscopy (AFS)

Table 1: Measured Hg(II) concentrations by P4VP-g-PVDF nanoporous membrane-electrodes in 2 ppb Hg(II) artificially polluted natural waters.

When SW samples were used raw (without filtration), the mercury recoveries were almost null for these samples. Two SW samples were studied after filtration and as raw samples (SW-4 and SW-5). For SW-4 and SW-5 the trials on filtrated samples and raw samples were performed the same days. For both samples, either filtrated or raw, the recovery was very low. It means that the ASV signal extinction is not due to suspended matter, but rather to the matrix composition and notably the total dissolved organic carbon. A high organic carbon content may favor sorption of Hg(II) dramatically decreasing the Hg(II) ion content. The sensors reported herein are only sensitive to free dissolved Hg^{2+} ions. This result suggests that the sorption of Hg(II) with dissolved organic species changes

the mercury speciation.

3.6 Prototype fabrication and function

A first generation prototype exhibiting its own integrated potentiostat, its software and set of membrane-electrode pads has been built (Figure 10). The manufacturing of membrane-electrode pads is cheap enough to use them as disposable products. A single-use avoids any memory effect of polluted membranes after Hg sampling. The membrane-electrode pads are thus consumables, well-adapted to be inserted by a simple clip to the probe. The prototype probe is composed of a ladel-like support and a measurement device driven by a dedicated software application.

Figure 10: Photograph of the prototype showing, immersed in a 125mL glass beaker container, a support holding the membrane-electrode pad. Membrane-electrode pads are connected to the measurement device *via* the support cable -inset: pad components, the membrane-electrode is sandwiched in middle where the open windows allow a permanent contact with the electrolyte. A dedicated software drives the overall system.

Regarding the measurement device, it is composed by seven sub-modules (Figure 11).The power supplies module is used to provide electronics needed power supplies, while the excitation module is used to generate the voltage, in the range from -2V to 2V, to be applied to the working electrode. An additional voltage measurement module is used to measure the voltage at the reference electrode. The current measurement module serves to measure the current between

the working electrode and the counter electrode in the range from nA to mA. The central unit and acquisition module allows the configuration of the voltage to be applied by the excitation module and also the data acquisition of the measurements of the voltage and current needed to make the voltammogram measurement. A data storage module is included to simply store the acquired data through a micro SD card. Finally, the communication module permits to send the data to a computer or to a smartphone application to visualize the data.

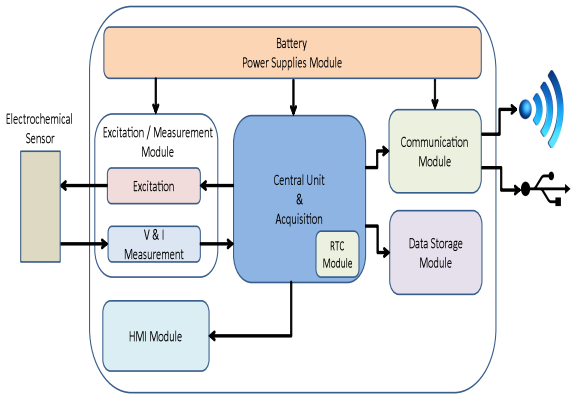

Figure 11: Scheme of sub-modules composing the measurement system of the prototype

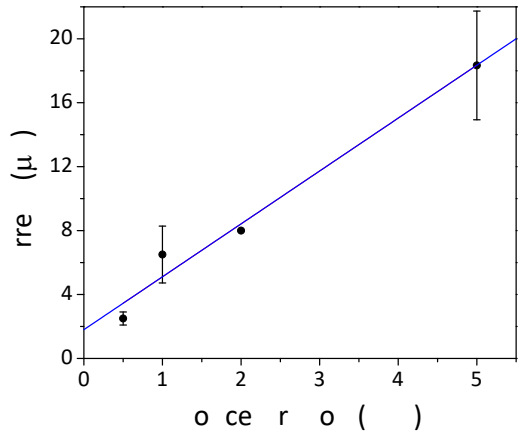

Figure 12: Calibration curve of Hg(II) using the prototype

Among devices available on the market, this specific device has the advantage to be portable and offer the possibility to perform on-site measurements. The device is simple to use and allows the registration of the voltammograms

in few minutes. End-users only have to plug the sensor to the device, power it on, open the software and click to start the measurement. A blue LED on the device turns on during the measurement, then end-users can obtain a voltammogram, save it as figure or export it as data table. Figure 10 shows the results obtained for Hg(II) detection using the device for different concentrations of Hg(II) and the Au-sputtered P4VP-g-PVDF membrane inserted in the pad (inset of Fig.8). Prior to measurement, the P4VP-g-PVDF membrane-electrodes have been immersed in diluted Hg(II) standard solutions following the aforementioned established protocol. As observed, the complete system presented a linear response *versus* Hg(II) concentration solution in ppb range.

3.7 Conclusions

Functionalized P4VP-g-PVDF nanoporous membrane-electrodes for anodic stripping voltammetry have been successfully fabricated and have exhibited a good sensitivity toward Hg(II) in deionized and natural waters. ~~The functionalized P4VP-g-PVDF nanoporous~~ Membranes were fully characterized by FTIR and by ~~a less conventional method based on~~ zeta potential determination. ~~The latter technique allows investigation of the quality of the nanopore coverage with P4VP chains by determining the charge state at the solid surface all along the cylindrical nanopores.~~ The zeta potential determination *via* the streaming potential was found to be a powerful technique to accurately characterize the charge state of functionalized organic nanopores. The isoelectric point of PVDF-g-P4VP nanoporous membranes was reached at pH 5 which corresponds to the pKa of P4VP. ~~It gave an elegant proof of dense P4VP grafting all along the nanopores.~~

To transform the radiografted P4VP-g-PVDF nanoporous membranes into ~~membrane-~~ electrodes, a thin gold layer of 35 nm was sputtered on both membrane surfaces. ~~The gold layer should be thin enough to not block the pore entry and thick enough to ensure a good conductivity. A gold layer of 35 nm was a good compromise and was used for all presented results.~~ The 3D nanostructuration of membrane-electrodes allowed a pre-concentration of mercury prior ASV measurement. Hg(II) adsorption isotherm displayed a Langmuir shape confirming that the adsorption of Hg(II) and P4VP was an equilibrium at room temperature. ~~It also informs about the limit of saturation of the radiografted membranes which starts at 10 ppb explaining the deviation from the linearity in all established calibration curves in ppb concentration range. Performances of the sensor were established in optimized conditions including 250 rpm ping-pong stirring, the use of 125 mL glass containers and triplicate measurements.~~ Using membrane-electrodes with a density of nanopores of $10^9 cm^{-2}$, an adsorption time of 4h into Hg(II) spiked deionized water , it resulted in a limit of detection of 0.1 ppb and mean precision of 20 %. ~~To get reliable results, it is recommended to run a calibration curve simultaneously with measurements in water samples to test.~~ It is important to mention that the membrane-electrodes are consumables and should be thrown away after use for quantitative results.

These ~~P4VP-g-PVDF~~ membrane-electrodes coupled with ASV sensoring showed a good mercury recovery in mineral waters and ground waters. However Hg(II) recoveries in surface waters were very low, even in filtrated samples. A relationship with total carbon content was pointed out. The sensors reported herein

are only sensitive to free dissolved Hg^{2+} ions. Future work should be done to cross our results with other techniques to understand how Hg(II) reacts with dissolved organic species and changes its speciation.
From the demonstrator home-made system, a first generation prototype exhibiting its own integrated potentiostat, its software and set of membrane-electrode pads was built. A calibration for Hg(II) in the range of 0-5 ppb was easily obtained with a reliable linearity.

3.8 Acknowledgements

This work belongs to CAPTOT project supported by the french National Agency for Research, ANR -Agence National de la Recherche- (grant ANR-15-CE04-13). The authors want to warmly thank the EMIR committee to have accepted their irradiation proposal and allow GANIL experiments. Notably, the strong implication of Dr. E. Balanzat and Dr. Y. Ngono-Ravache during swift heavy ion irradiations is herein acknowledged. The authors are also grateful to Sébastien Ceste from Centre Polymedia of the Ecole Polytechnique (France) for its graphic work implication.

References

[1] D. Martin-Yerga, M.B. Gonzalez-Garcia, A. Costa-Garcia, Electrochemical determination of mercury: A review, Talanta 116 (2013) 1091-1104. https://doi.org/10.1016/j.talanta.2013.07.056

[2] M. Barsbay, O. Guven, T.L. Wade, M-C. Clochard, Functionalized membrane electrodes (FMEs) by RAFT-mediated radical polymerization inside synthetic nanochannels, J. Memb. Sci. 445 (2013) 135-145. https://doi.org/10.1016/J.memsci.2013.05.029

[3] Y. Bonfil, M. Brand, E. Kirowa-Eisner, Trace determination of mercury by anodic stripping voltammetry at the rotating gold electrode, Analytica Chimica Acta 424 (2000) 65-76. https://doi.org/10.1016/S0003-2670(00)01074-6

[4] A. Giacomino, O. Abollino, M. Malandrino, E. Mentasti, Parameters affecting the determination of mercury by anodic stripping voltammetry using a gold electrode, Talanta 75 (2008) 266-273. https://doi.org/10.1016/j.talanta.2007.11.015

[5] A. Mandil, L. Idrissi, A. Amine, Stripping voltammetric determination of mercury(II) and lead(II) using screen-printed electrodes modified with gold films and metal pre-concentration with thiol-modified magnetic particles, Microchim. Acta 170 (2010) 299-305. https://doi.org/10.1007/s00604-010-0329-x

[6] K. Zinoubi, H. Majdoub, H. Barhoumi, S. Boufi, N. Jaffrezic-Renault, Determination of trace heavy metal ions by anodic stripping voltammetry using nanofibrillated cellulose modified electrode, J. of Electroanal. Chem. 799 (2017) 70-77. https://doi.org/10.1016/j.jelechem.2017.05.039

[7] P. Guan, P.R. Guo, N. Liu, F. Zhang, Y.Q. Lei, The preparation of a flexible AuNP modified carbon cloth electrode and its application in electrochemical detection of Hg(II) by continuous flow in environmental water, Analyst 143 (2018) 18, 4436-4441. https://doi.org/10.1039/c8an01284a

[8] Y. Mollamahale, M. Ghorbani, A. Dolati, M. Ghalkhani, M. Application of 3D gold nanotube ensembles in electrochemical sensing of ultra-trace Hg(II) in drinkable water, Surfaces and Interfaces 10 (2018) 27-31. https://doi.org/10.1016/j.surfin.2017.11.001

[9] F. Tan, L. Cong, N.M. Saucedo, J. Gao, X. Li, A. Mutchandani, An electrochemically reduced graphene oxide chemiresistive sensor for sensitive detection of Hg^{2+} ion in water samples, Journal of Hazardous Materials 320 (2016) 226-233. https://doi.org/10.1016/j.jhazmat.2016.08.029

[10] A.M. Ashrafi, Z. Koudelkova, E. Sedlackova, L. Richtera, V. Adam, V., Review - Electrochemical sensors and biosensors for determination of mercury ions, Journal of Electrochemical Society 165 (2018) 16, B824-B834. https://doi.org/10.1149/2.0381816jes

[11] W.Q. Tang, L.H. Mao, Z.F. Zhou, C.F. Wang, Q.L. Chen, S. Chen, S., Facile synthesis of 4-vinylpyridine-based hydrogels via laser-ignited frontal polymerization and their performance on ion removal, Colloid. Polym. Sci. 292 (2014) 2529-2537. https://doi.org/10.1007/s00396-014-3279-8

[12] D.D. Maksin, S.O. Klajajavic, M.B. Dolic, J.P. Markovic, B.M. Ekmescic, A.E. Onjia, A.B. Nastasovic, Kinetic modeling of heavy metal sorption by vinyl piridine based copolymer, Hem. ind. 66 (2012) 6, 795-804. https://doi.org/10.2298/HEMIND121002112M

[13] P. Viel, S. Palacin, F. Descours, C. Bureau, Electropolymerized poly-4-vinylpyridine for removal of copper from wastewater, Appl. Surf. Sci. 212-213 (2003) 792-796. https://doi.org/10.1016/S0169-4332(03)00105-3

[14] H. Bessbousse, J-F. Verchere, L. Lebrun, Increase in permeate flux by porosity enhancement of a sorptive UF membrane designed for the removal of mercury(II), J. Memb. Sci. 364 (2010) 167-176. https://doi.org/10.1016/j.memsci.2010.08.018

[15] H. Bessbousse, T. Rhalou, J-F. Verchere, L. Lebrun, Novel metal-complexing membrane containing poly(4-vinylpyridine) for removal pf Hg(II) from aqueous solution, J. Phys. Chem. B 113 (2009) 8588-8598. https://doi.org/10.1021/jp900863f

[16] B.L. Rivas, H.A. Maturana, M. Luna, Selective binding of mercury ions by poly(4-vinylpyridine) hydrochloride resin, J. Appl. Polym. Sci. 74 (1999) 1557-1562. https://doi.org/10.1002/(SICI)1097-4628(19991107)74:6¡1557::AID-APP30¿3.0.CO;2-2

[17] Z. Li, S. Xia, J. Wang, C. Bian, J. Tong, J., Determination of trace mercury in water based on N-octylpyridium ionic liquids preconcentration and stripping voltammetry, Journal of Hazardous Materials 301 (2016) 206-213. https://doi.org/10.1016/j.jhazmat.2015.08.061

[18] H. Bessbousse, N. Zran, J. Faul, B. Godin, V. Lem T. Wade, M-C. Clochard, Poly(4-vinylpyridine) radiografted PVDF track etched membranes as sensors for monitoring trace mercury in water, Rad. Phys. Chem. 118 (2016) 48-54. https://doi.org/10.1016/j.radphyschem.2015.03.011

[19] P. Braunstein, M.T. Camellini, Competing Metal-Metal bonding in hetetrometallic complexes of gold and mercury. Synthesis of contrasting Fe-Au-Au-Fe and Fe-Hg-Fe complexes, Inorg. Chem. 31 (1992) 3685-3687. https://doi.org/10.1021/ic0004a002

[20] J.L. Parker, N.S. Bloom, Preservation and storage techniques for low-level aqueous mercury speciation, Science of the Total Environment 337(2005) 1, 253-263. https://doi.org/10.1016/j.scitotenv.2004.07.006

[21] M.B. Andersen, H. Bruus, J.P. Bardhan, J. P., S. Pennathur, S. Streaming current and wall dissolution over 48 h in silica nanochannels, J. Colloid Interface Sci. 360 (2011) 262- 271. https://doi.org/10.1016/j.jcis.2011.04.011

[22] H. Wang, I.H. Lee, M. Yan, A general method to determine ionization constants of responsive polymer thin films, J. Colloid and Interface Sci. 365 (2012) 178-183. https://doi.org/10.1016/j.jcis.2011.08.081